Environmental Science Nano

ROYAL SOCIETY OF CHEMISTRY

PAPER

View Article Online
View Journal | View Issue

Cite this: *Environ. Sci.: Nano*, 2026, **13**, 447

Oxidation *vs.* agglomeration: impact of graphene oxidation on self-interactions and PFAS capture

Caitlin G. Bresnahan,* Timothy C. Schutt and Manoj K. Shukla

Per- and polyfluoroalkyl substances (PFAS), also known as "Forever Chemicals", are a class of compounds characterized by their extremely stable C–F bonds. These molecules possess desirable properties, which has led to their widespread use in industry and household products. PFAS have been found in waterways around the world. This is concerning because PFAS have also been found to have negative health impacts on the human population. It is essential that effective adsorbent materials are developed to remove PFAS from the environment. Carbon nanomaterials such as graphene oxide are often used for water remediation and filtering purposes. Pure graphene is hydrophobic, but the presence of hydroxyl, epoxy, and carboxyl groups increases its hydrophilicity. Meanwhile, PFAS have hydrophobic tail groups and hydrophilic head groups. This work is focused on determining how the extent of oxidation in graphene oxide impacts the capture of amphiphilic PFAS. Seven graphene oxide flakes are examined which contain an oxygen coverage of 0.0, 2.4, 5.2, 7.6, 10.9, 14.5, and 17.5% oxygen by mass. In addition to becoming more hydrophilic as the oxygen content increases, the self-interaction between flakes also changes. Both factors play a role in how the materials interact with PFAS. Graphene oxide flakes with 5.2% and 7.6% oxygen by weight exhibited the highest PFAS-affinity out of all flakes studied herein.

Received 7th August 2025,
Accepted 22nd November 2025

DOI: 10.1039/d5en00731c

rsc.li/es-nano

Environmental significance

Per- and polyfluoroalkyl substances (PFAS), otherwise known as "Forever Chemicals", are a class of contaminant that has received much attention in the last few years. Their properties make them ideal for industry and many applications; however, studies have repeatedly found that PFAS have negative health impacts on humans and are highly persistent in the environment. It is essential to remove PFAS from waterways, but this is a difficult challenge as the unique properties that make PFAS beneficial also make them uniquely hard to capture and degrade. This work has investigated the ideal oxidation level of graphene oxide for optimal PFAS binding in water, paving the way for developing new carbon nanomaterials for PFAS remediation. In particular, this study sheds light on the interplay between PFAS interaction with graphene oxide flakes and flake–flake self-interaction. It also illustrates how these factors can be manipulated to increase PFAS capture from water.

1. Introduction

Per- and polyfluoroalkyl substances (PFAS) are molecules that are characterized by their interesting and unique properties. They are formed by replacing C–H bonds with C–F bonds in organic compounds, which changes their properties such that they become extremely stable.[1–3] Their fluorine tails make them oleophobic and hydrophobic; meanwhile the presence of the hydrophilic anionic headgroup makes the species amphiphilic.[1–3] The electronically dense fluorine molecules can shield the alkyl chain, making degradation difficult.[2] Thus, fluorinated compounds have been developed to exploit these properties for use in many industries including electronics, metal coatings, aqueous firefighting foams, food packaging, automotive, semiconductors, medical applications, and aerospace, as well as in common household products like cleaning supplies, toilet paper, and cosmetics.[2–8] While their melting and boiling points are dependent on chain length, short chain PFAS have melting points that range from 0–100 °C and boiling points between 100 and 150 °C.[2] Further, short chain PFAS have higher solubility and can spread easily through environmental matrices.[2] Their resistance to degradation combined with their high mobility in the environment has led to PFAS being detected worldwide, including remote locations like the Arctic.[9–13] PFAS can leach from landfills and industry, and spread through atmospheric pathways, soils, solid waste, and waterways.[2,10–14] Humans are exposed to PFAS through air pollution, diet, contaminated water, and consumer products.[7,11] Unfortunately, PFAS have been shown to have

Engineer Research and Development Center, Environmental Laboratory, US Army Corps of Engineers, Vicksburg, MS 39180, USA.
E-mail: Caitlin.G.Bresnahan@usace.army.mil

negative effects on human health including impacts on reproductive hormones, breast milk, vaccine response, kidney disorders, and some cancers.[7,15–21]

Given the widespread usage, contamination, and potential health implications of PFAS, it is essential to address the removal of PFAS from the environment. PFAS removal is difficult because thousands of PFAS exist, they are very mobile, they are amphiphilic, and they have strong C–F bonds.[1,22] Several materials have been examined with varying degrees of success for PFAS capture including clays,[23–27] activated carbon,[28–33] modified cellulose,[34–36] anion exchange resins,[37–39] zeolites,[40–42] metal organic frameworks,[43–46] covalent organic frameworks,[46–48] hydrogels,[49–51] and cyclodextrin[52,53] materials.[9,54,55] Many of these materials have been chosen due to their modifiable functionality and properties. Increasingly, carbon nanomaterials such as graphene and its functionalized derivatives have been examined for PFAS removal.[56–64] Lamb *et al.* used computational methods to examine how PFAS bind to a graphene sheet.[60] They explored the aggregation of PFAS at the surface of the sheet at neutral and acidic pH. Shrestha *et al.* studied how using an alternating current can lead to reversible adsorption of PFAS to graphite.[56] Several modifiable functionalized graphene materials have been examined for improved PFAS removal. Mahpishanian *et al.* studied improvements to PFAS capture with magnetic amine functionalized graphene oxide.[64] Lath *et al.* created an iron oxide modified reduced graphene oxide composite that performed well for PFAS removal.[65] Trifoglio *et al.* examined adding alkyl chains that were polar, charged, and hydrophobic to measure the impact on PFAS adsorption.[61] Our previous work examined different functionalities (graphene, graphene oxide, partially fluorinated graphene flakes, fully fluorinated flakes, and amine functionalized flakes) and found that PFAS capture involved an interplay between flake functionality and flake–flake clustering.[62] In our subsequent work, we examined how adding alkyl chains to graphene oxide would affect PFAS capture through ideal flake clustering.[63] The addition of the alkyl chains impacted clustering mechanisms to increase PFBA capture. This indicates that flake–flake aggregation is a parameter than can be tuned through functional modifications of the graphene oxide to optimize PFAS capture.

One unresolved factor in the field of PFAS adsorption revolves around the mechanisms by which PFAS are ideally captured. Leung *et al.* stated that the potential interactions include electrostatic, hydrophobic, π–π, fluorophillic, hydrogen bonds, ion exchange, ion bridging, and van der Waals interactions.[1] Most studies in the literature have found that the dominant interactions between PFAS and adsorbents are electrostatic and/or hydrophobic interactions.[1,26–29,54,66,67] The debate revolves around whether electrostatic or hydrophobic interactions drive PFAS adsorption. It appears that the answer is dependent on the adsorbents used and target PFAS. Willemsen *et al.* looked at PFAS binding to smectite clay and found that adsorption occurred on the hydrophobic portions of the clay.[26] Park *et al.* found that the hydrophobic interactions played a major role in PFAS adsorption to activated carbon.[28] Fabregat-Palau *et al.* found that carbon materials capture PFAS predominantly through hydrophobic interactions.[67] On the other hand, Cantoni *et al.* looked at PFAS adsorption to activated carbon, and found that the role of electrostatics was integral for PFAS removal.[29] Dong *et al.* modified clays with ionic liquids, and found that electrostatics were the predominant interaction with PFAS.[27] However they also found that the hydrophobic interactions contributed more as the PFAS chain length increased.

In this work, we explore the interplay between electrostatic and hydrophobic effects for PFAS capture at the molecular level through simulations of graphene oxide with varying levels of oxidation. Findings uniquely highlight mechanisms of flake aggregation and binding site quality as competing factors in PFAS capture using graphene oxides. Graphene oxide has shown promise for removing contaminants from water.[68,69] It has ideal features including amphiphilic properties,[70,71] has been shown to bind amphiphiles,[72] is easily synthesized and modifiable,[68] and has a high surface area.[68] The extent of oxidation on graphene oxide can be controlled through parameters within its synthesis method, such as the amount of oxidizing agent used.[68,73–75] Wang *et al.* examined varying oxidation of graphene oxide for binding PFOA with computational methods.[57] They used a graphene oxide slab with water and one PFOA molecule. They varied the number of hydroxyl groups of their graphene oxide slab. They found that PFOA adsorbed best to graphene, and that the PFOA interaction decreased as oxidation increased. In this work, we examined how flake clustering and PFAS adsorption is impacted by varying the level of oxidation on the graphene oxide flakes. We explored an under-studied regime of graphene oxide flakes with low oxygen coverage of 0.0, 2.4, 5.2, 7.5, 14.5, and 17.5% oxygen by mass. We found the degrees of oxidation that optimize the competing effects of the hydrophobicity of the flake backbone, and the electrostatic interaction capacity of the functional groups to adsorb PFAS. The number of epoxide and hydroxyl groups are varied to match experimental proportions. In each simulation we included 5 flakes, 5 molecules of perfluorooctane sulfonate (PFOS), five molecules of perfluorooctanoic acid (PFOA), and five molecules of perfluorobutanoic acid (PFBA). These simulations allowed us to elucidate: (i) how long and short chain PFAS compete for the graphene oxide flakes based on the hydrophobicity of the flake, (ii) how the PFAS headgroup impacts adsorption through the competition of favorable and unfavorable electrostatic interactions and (iii) how flake–flake clustering impacts PFAS adsorption, providing valuable insight into the mechanisms of PFAS capture. We find that there is an ideal oxygen coverage for PFAS capture at 5.2% and 7.6% oxygen by weight. Importantly, we show how capture is impacted by flake

clustering, elucidating physical parameters which can be tuned to enhance PFAS capture.

2. Methods

This work used a test set of three PFAS: PFOS, PFOA, and PFBA. All were considered in their anionic form, because this form tends to be more prevalent at environmentally relevant pH values.[2] The test set has short and long chain PFAS. Carboxylic acid and sulfonic acid head groups are both represented. In order to determine the impact that the extent of oxygen coverage on graphene oxide has for PFAS capture, seven flakes were generated. In our initial work, a graphene oxide flake was built to be 10.9% oxygen by weight and have dimensions of 30 × 40 Å^2 (referred to herein as GOX 10.9, Fig. 1).[62] Further, pure graphene (referred to herein as GNX) was made by removing all oxygen groups from GOX 10.9. The edges of the flakes were terminated with a hydrogen border to satisfy the edge valency. Both flakes are used in this study to track trends in increasing oxygen levels. The number following GOX indicates the percent oxygen by weight of the flake. GOX 2.5, GOX 5.2, and GOX 7.6 were generated by randomly removing functional groups from GOX 10.9, while GOX 14.6 and GOX 17.5 were built by randomly adding functional groups. Fig. S1 in the SI contains images of the full flake (front, back, and side view) for each level of oxygen coverage.

Table S1 shows how many hydroxyl, epoxy, and carboxyl groups are present on each graphene oxide flake. The literature shows that graphene oxide has a C/O ratio ranging from 30 to 2.2.[76–78] Every graphene oxide structure fits in the experimental C/O ratio except for GOX 2.4. Its C/O ratio is 53.6, which is higher than the literature values. GOX 2.4 was included to have a complete view of the reduction of the flakes, though this structure would be difficult to obtain experimentally. For each graphene oxide flake examined, a 90 × 90 × 90 Å^3 cubic box was filled with 5 flakes, 5 of each PFAS, 15 sodium counter ions, and water. The number of PFAS and flakes were chosen to model capture at conditions below the saturation point of the sorbent material and minimize the PFAS–PFAS interactions for a straightforward analysis, while also allowing for adequate sampling to effectively probe how the oxidation level affects PFAS capture. Table S2 shows the number of each molecule type for each simulation set. The generalized Amber force field (GAFF) force-field was used to describe PFAS and flakes.[79] The same parameters and point charges used on the functional groups in our previous work were used herein.[62] The total charge of the flake was then distributed as point charges over the remaining carbons of the flake to obtain a net zero charge over the flake. TIP4P-Ew was used to describe water molecules.[80–82]

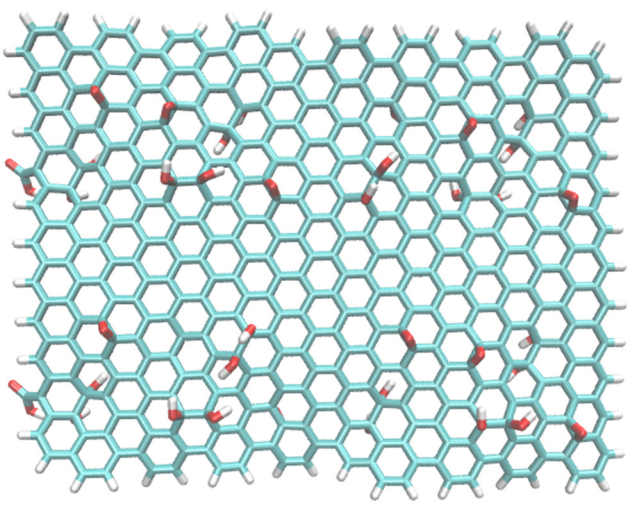

Fig. 1 Molecular structure of GOX 10.9.

Twelve starting configurations were generated for each graphene oxide flake using Packmol.[83] Packmol randomly places molecules in the box, and thus 12 independent simulations were executed. Having 12 replicas allows for broad sampling and inclusion of confidence intervals for data analysis. All simulations were executed in the AMBER suite of packages.[84] NPT equilibrium simulations at a pressure of 1 atmosphere allowed for the relaxation of the initial starting configuration and for the box to converge the density. Once equilibrium was reached, production runs were executed in the NVT ensemble at 300 K for 100 ns with Langevin dynamics and a timestep of 2 fs.[85] The SHAKE algorithm was used to constrain hydrogen bonds.[86] It takes time for the flakes to agglomerate and for PFAS to reach the flakes. As such, the analysis was performed on the last 50 ns of the simulations. The CPPTRAJ toolkit was used to calculate various properties such as the number of contacts, linear interaction energies (LIE), Connolly surface areas, and radial distribution functions (RDFs).[87,88] Visual Molecular Dynamics software was used to visualize trajectories and generate images.[89]

3. Results and discussion

3.1. PFAS–flake interactions

In order to quantify the PFAS–flake interactions, the linear interaction energy (LIE) was calculated. LIE is the sum of electrostatic and van der Waals contributions between interacting species. Fig. 2 depicts the LIE of PFAS with each flake. The LIE is normalized by the molecular mass of the PFAS. This accounts for the size effects of the various PFAS. Normalizing the LIE makes the work more comparable to experiments and regulations where concentrations are often given on a per-mass basis (*i.e.* ng L^{-1}, ppt) where partitioning is with respect to the mass of the contaminant. Error bars show the standard deviation between 12 independent simulations. Different starting configurations of the graphene oxide flakes result in different aggregate structures as the flakes coalesce. Replicates within an oxidation level exhibit similar motifs in stacking overlaps and surface areas exposed. Variation in the binding interactions stems from sampling

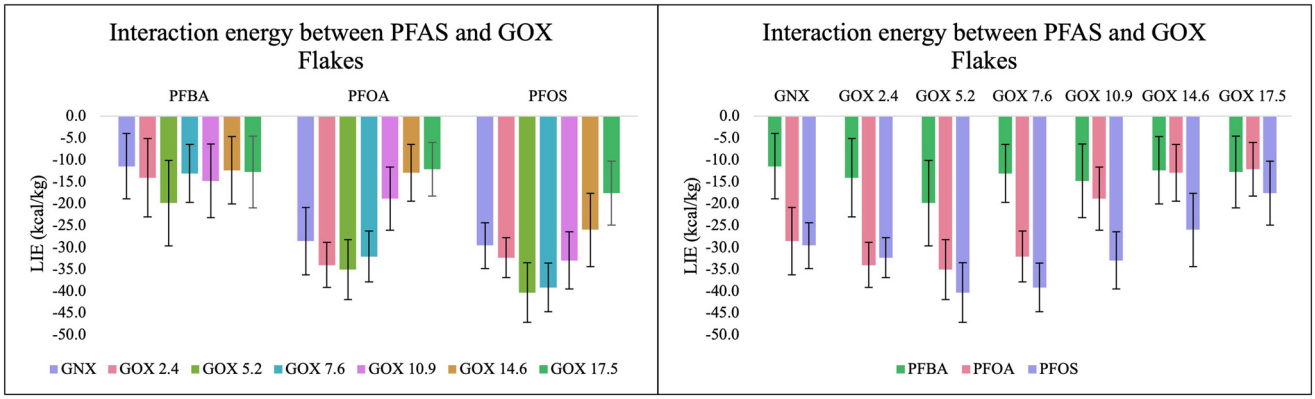

Fig. 2 Linear interaction energy between the PFAS and GOX flakes. Left panel – data is sorted by PFAS. Right panel – data is sorted by graphene flake. All LIEs are given in kcal kg^{-1} of PFAS.

numerous different orientations and sites for PFAS adsorption. Large error bars are expected because there are many different ways for each type of PFAS and flake to interact in the simulation. Small changes in bonding orientation can cause large changes in LIE. Moreover, PFBA is very mobile in all simulations and thus has very large error bars.

Several trends can be observed based on the data shown in Fig. 2. For all PFAS under investigation, the LIE becomes more negative (an increase in favorability) from GNX to GOX 5.2. After the oxygen level is increased to 10.9% oxygen by weight, the LIE trends towards less favorable interactions with increasing graphene oxidation. At lower oxygen coverages, the hydrophobic effects dominate (through flake–flake aggregation and the PFAS tail over the flake), but as the oxygen coverage increases electrostatics begin to play a more important role (as will be discussed in more detail below). Thus, the LIE indicates that there is an ideal oxygen coverage for capturing long chain PFAS at around 5.2% and 7.6% oxygen by weight. This is in contrast to Wang *et al.* who found that the PFOA had the strongest interaction with pure graphene, and the interaction decreased with increasing oxygen.[57] However, that simulation had one PFOA and a graphene oxide slab. In systems with more than one graphene surface, the oxidation level impacts how the flakes aggregate and the surface area that is available for interaction, and thus PFAS binding. This work includes several flakes of the same type with very low oxidation levels (GOX 2.4–GOX 7.6) in the simulations.

Our previous work, which only included GNX and GOX 10.9, did not show much aptitude for graphene oxide to capture PFOA. PFOA is generally more difficult to capture than PFOS due in part to its higher solubility in water. However, this work shows a clear and strong improvement in PFOA capture capabilities at low oxygen coverage (2.4% to 7.6% oxygen by weight). The lower oxygen coverage graphene oxide flakes have larger hydrophobic domains than the 10.9% oxygen flakes. The 5.2% and 7.6% oxygen flakes also have significantly more solvent-accessible surface area than GNX or 2.4% oxygen flakes. If the flake has sufficient hydrophobic surface and exposes binding sites through dispersed aggregation, as is the case GOX 2.4–GOX 7.6, the high solubility of PFOA can be overcome and achieve high degrees of adsorption. When the oxygen content is greater than or equal to 10.9%, the LIE for PFOA with GOX appears less favorable with the increase in oxidation of the graphene. At this point, the electrostatic interactions begin to take over and PFOA water solubility dominates. Similarly, PFOS binding affinity for GOX is less favorable at 10.9% oxygen by weight. However, the weakening in LIE is more gradual, meaning PFOS capture performance is not hindered as quickly by the increase in oxygen coverage. This is in accordance with the lower solubility of PFOS compared to PFOA.[90,91] At 10.9% oxygen content and above, many of the hydrophobic binding sites on the graphene oxide are somewhat obstructed by polar functional groups. For PFOS, these mediocre binding sites are still thermodynamically favorable compared to solvation in bulk water. In contrast for PFOA, the tighter charge localization of PFOA around the head group and slightly smaller overall molecular size of PFOA compared to PFOS mean that PFOA is more sensitive to even minor obstructions of binding sites and slight over-oxidation can be enough to prohibit large percentage of PFOA from binding. This is in line with the experimental findings of Fabregat-Palau *et al.*[67] who observed *via* changes in response to tail length that hydrophobic interactions were the most important followed by electrostatic interactions in determining adsorption efficiency of PFAS to biochars.

It will be informative to look at the electrostatics of the flakes to explain why PFAS binding strength grows to a point, and then starts to decrease again. Fig. 3 shows the oxidized flakes colored by charge. Fig. S2 shows the histogram of charge counts per flake. The charges for functional groups, secondary, and tertiary atoms are set based on RESP mapping of DFT calculations and the total charge is normalized over the remaining carbons, as described in the methods. Thus, as can be seen in Fig. 3, the increase in the oxidation level leads to an increase in the number of electronegative functional groups present. In response, the graphene carbons become more positive to accommodate the overall neutral charge of the flake. GNX and GOX 2.4 have the fewest oxygen

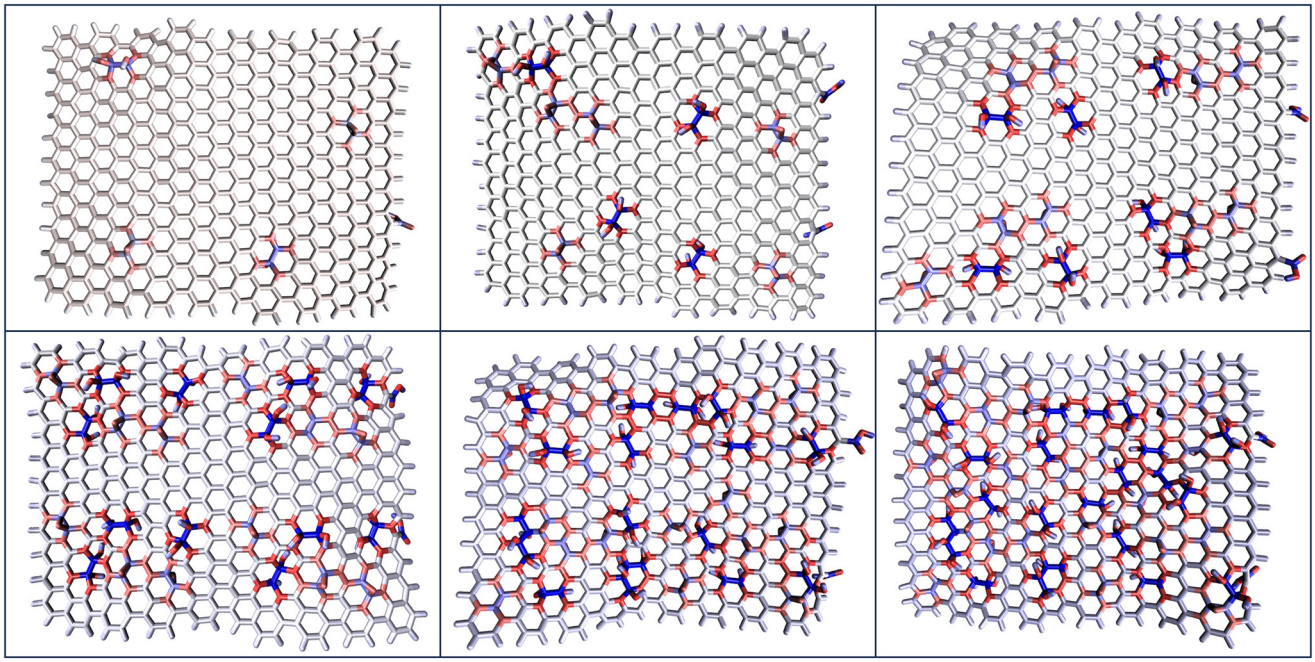

Fig. 3 Oxidized graphene flakes colored by charge. Red indicates negative charge, white is neutral, blue is positively charged. From left to right: top row – GOX 2.4, GOX 5.2, GOX 7.6 bottom row: GOX 10.9, GOX 14.6, GOX 17.5.

atoms and the carbon backbone is largely neutral with an area for the flakes to stack with each other *via* hydrophobic aggregation, minimizing the surface area available for PFAS binding. GOX 5.2 and GOX 7.6 have pockets of charge density and pockets of nearly neutral carbon backbone. This allows for the PFAS head groups to be stabilized by the pocket of positive charge of the hydrogen on the OH group, and the carbon directly attached to the OH group while the PFAS tail group can lay over the neutral carbon backbone, through hydrophobic effects. The charged pockets take up more space on the flake as the level increases. Therefore, two factors will hinder PFAS binding. Firstly, the positively charged portions of the flake are more difficult to reach, as the negatively charge portions get closer together and repel the headgroup of the PFAS. Secondly, the backbone becomes more positively charged which hinders the hydrophobic aggregation of the PFAS tail to the flake. These factors work in tandem to prevent PFAS binding.

With respect to GNX and GOX 2.4, PFOA and PFOS have strong and equivalent interactions with the flakes, while PFBA has very little interaction. At these low oxidation levels, the nonpolar aggregation between the PFAS tail group has the dominant effect for PFAS capture. Both PFOA and PFOS have an 8-carbon long tail compared to PFBA which has only 4 carbons. Moreover, PFBA has the highest water solubility, and thus is more difficult to capture.[91] For GOX 5.2 and GOX 7.6, PFOS has a stronger LIE for the flakes than PFOA. By 10.9% oxygen by weight, PFOA affinity has decreased drastically and is on par with the PFBA–flake interactions. This shift arises because the degree of electrostatic interactions diminishes the number and access to hydrophobic surface areas of the flake. While the LIE is less favorable for PFOS after 10.9% oxygen by weight, it still has a clear affinity for the flakes. By GOX 17.5, the LIE between PFOS and the flake is on par with that of PFOA and PFBA. The hydrophobic domains are virtually non-existent and the water solubility of the PFAS is thermodynamically preferred over adsorption to the flake. The number of contacts between the PFAS and flakes is shown in Fig. S2, and it shows the same trends described above.

Fig. 4 shows snapshots of the last step for three replicas of the simulations. The snapshots help illustrate how these trends occur. For GNX, GOX 2.4, and GOX 5.2, all PFOS and PFOA are near the graphene flakes while PFBA is largely found in solution. For GOX 7.6 all PFOS, PFOA, and some PFBA are near the flakes and thus fewer PFBA molecules are found in solution than in the lower oxygen level flakes. There is a balance between electrostatic forces to capture PFBA while maintaining a hydrophobic area on the flake for non-polar interactions with the PFBA tail. With the oxidation levels increasing to GOX 10.9–GOX 17.5, all PFAS have revealed less affinity for the flakes.

3.2. Flake–flake interactions

In our previous work, we showed that PFAS capture by functionalized graphene oxide flakes was dependent on the type of functionalization as well as the clustering of the flakes.[62] It is well known that graphene is hydrophobic and interacts with itself. Adding oxygen groups increases the hydrophilicity of the flakes. Fig. 4 shows that the flakes still cluster together at every level of oxidation examined. Fig. 5

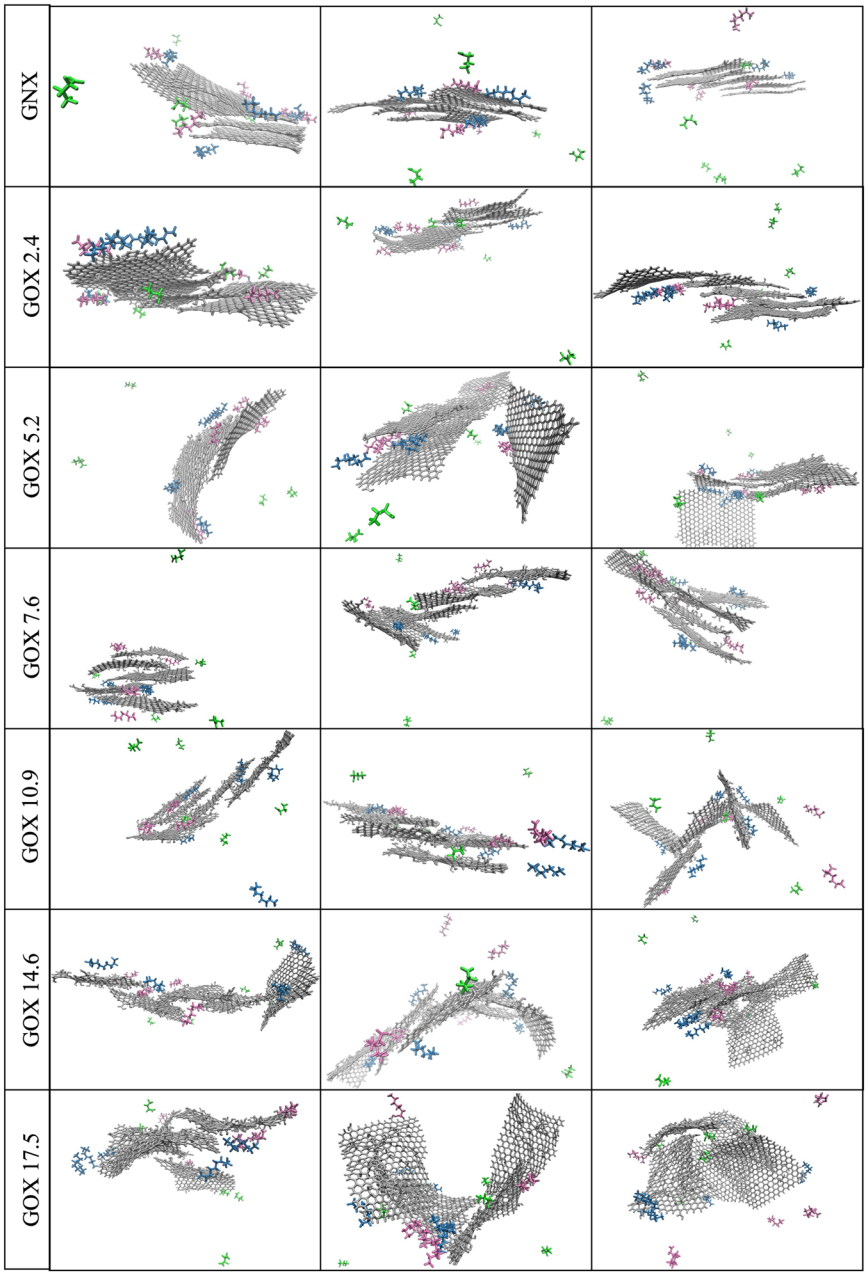

Fig. 4 Snapshots of the last step of simulations for three configurations. PFBA is indicated in green, PFOA in pink, and PFOS is in blue.

shows the LIE of the flake–flake interactions normalized by the mass of the flake, and the surface area of the agglomerated flakes. On the timescales of MD, the flakes will aggregate and stay aggregated indefinitely in whatever lowest energy configuration was reached during relaxation dynamics of the initial random packing. Therefore, the surface area of the flakes was calculated for the last step of the simulation, and then averaged over all twelve configurations for each flake type. Simulations were executed on GOX 7.6 (12 replicas) without PFAS to estimate the impact of PFAS on flake aggregation. The results are shown in section S5. Our results show that at this concentration, the presence of PFAS does not impact flake aggregation.

GNX has a very strong LIE with itself. The flakes are stacked, and thus the available surface area for PFAS to interact with is low. As the level of oxygen on the flake increases the flake–flake LIE decreases. The flakes begin to interact more with the surrounding water and less with each other as oxygen on the flake increases. This is intuitive, examining the electrostatics in Fig. 3. The lower oxidized flakes have less polar electrostatics and a nearly neutral carbon backbone that is vast for hydrophobic aggregation between flakes to occur. As the oxidation increases, the extent of polar electrostatics increases, and thus the flake can interact with water more readily. This trend mirrors the findings of Liu *et al.*[77] and others who

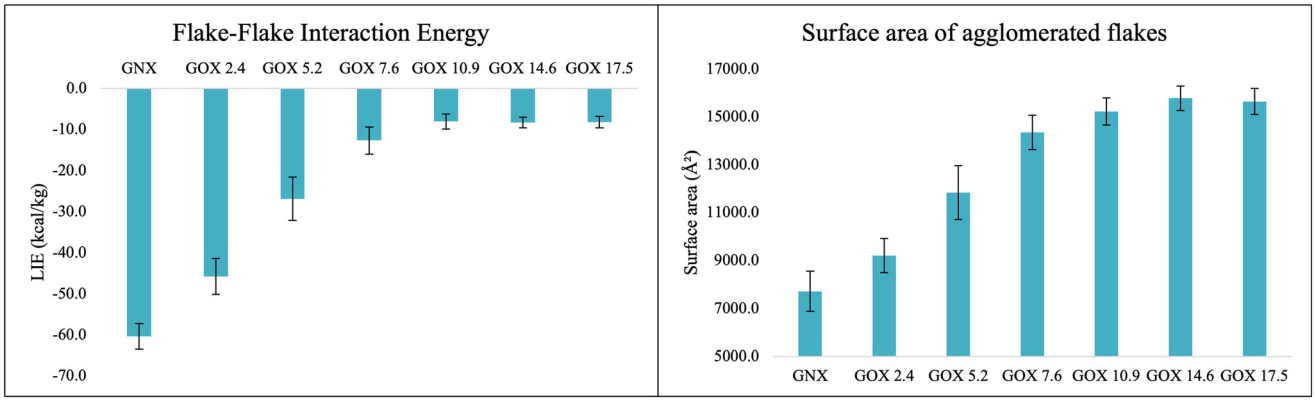

Fig. 5 The left panel shows the flake–flake LIE normalized by the molecular weight of the flake. The right panel shows the surface area of the agglomerated flakes.

report experimental difficulties in dispersing lowly-oxidized graphene sheets due to excessive hydrophobic aggregation. The LIE plateaus at 10.9% oxygen by weight, at around −8.0 kcal kg^{-1}. Commensurately, the surface area of the agglomerated flakes increases as the amount of oxygen on the flake increases. The surface area plateau is also reached at GOX 10.9. Fig. 6 shows a snapshot from the last step of three configurations of the simulations. This figure depicts the progression of flake clustering as oxygen coverage increases. GNX has tightly stacked flakes. In GOX 2.4, the flakes start to spread out incrementally, having less overlap between the flakes than GNX. By GOX 5.2 the flakes have spread out more, but the main interaction between flakes comes from stacking of the hydrophobic carbon backbone. The GOX 7.6 flakes have spread out to where the functional groups on one flake are interacting with other flakes, causing separation between the hydrophobic parts of the flakes and decreasing the tight stacking motif. As the oxygen level rises from 10.9% oxygen by weight to GOX 17.5, the flakes begin interacting with each other predominantly through functional group/electrostatic interactions rather than carbon backbone stacking.

At 5.2% oxygen by weight, the minimal oxygen coverage allows for the hydrogen border edges of the flakes to interact with the functional groups on the surface of the flakes and for carbon backbone stacking to occur. These interactions create shelves where the PFAS head group can interact with the hydrogen border (the hydrogen terminated edges of the graphene flake), while the PFAS tail group has a hydrophobic surface to lay over. Fig. 7 shows a snapshot example of this binding mode. The flakes are off-set stacked – meaning they are stacked, but not as rigidly as GNX.

GOX 7.6 allows for the head group of PFAS to interact with functional groups on the surface of the flake, as well as creating edges like in GOX 5.2, and continues to increase the surface area for potential adsorption while maintaining a hydrophobic backbone for the interaction of the tail group of the PFAS. When the oxygen level is greater than or equal to 10.9% oxygen by weight, the hydrophilic functional groups (and thus, electrostatic effects) begin to outweigh the available hydrophobic carbon backbone patches, reducing the available surface area for interaction with the PFAS tail resulting in decreased PFAS capture. This mechanism is further confirmed in subsequent sections. Moreover, Fig. S3 shows the water–flake interactions and water–PFAS interactions which further support that the exposed surface area is maxed out.

3.3. Carbon backbone RDFs

Radial distribution functions (RDFs) were calculated for the head and tail group of PFAS to all functional groups of the graphene oxide flakes. These RDFs allow us to understand how PFAS are distributed around distinct functionalities including the hydrophobic carbon backbone, hydroxyls, and edges of each of the GOX Flakes. We start with RDFs between PFAS and the hydrophobic carbon backbone portions of the GOX flakes. The head group was designated as the initial carbon (for carboxylate head groups – carbon attached to the oxygen atoms, for sulfonate – carbon attached to SO_3^-). The tail group was designated as the terminal carbon. Herein the RDFs most relevant to PFAS binding are discussed while all other RDFs are located in Fig. S4 to S6. Fig. 8 illustrates the RDFs of PFAS head and tail groups to the carbon backbone of the flakes.

The carbon backbone is defined as any carbon that is not attached to a functional group, or adjacent to a carbon that is attached to a functional group. These carbons make up the hydrophobic domains of the flake. This definition of the carbon backbone will lead to wide peaks (see Fig. 3 to view the wide area of hydrophobic patches). Larger RDF values indicate higher localized adsorption. In general, the RDFs in Fig. 8 align with the interaction strength results in Fig. 2 for the same functional reasons described in previous sections. The PFAS adsorption to flakes increases as oxidation increases to 5.9% and 7.6% oxygen by mass. Adsorption then decreases as oxygen coverage increases further. On these flakes, PFOS adsorbs the most followed by PFOA, and lastly,

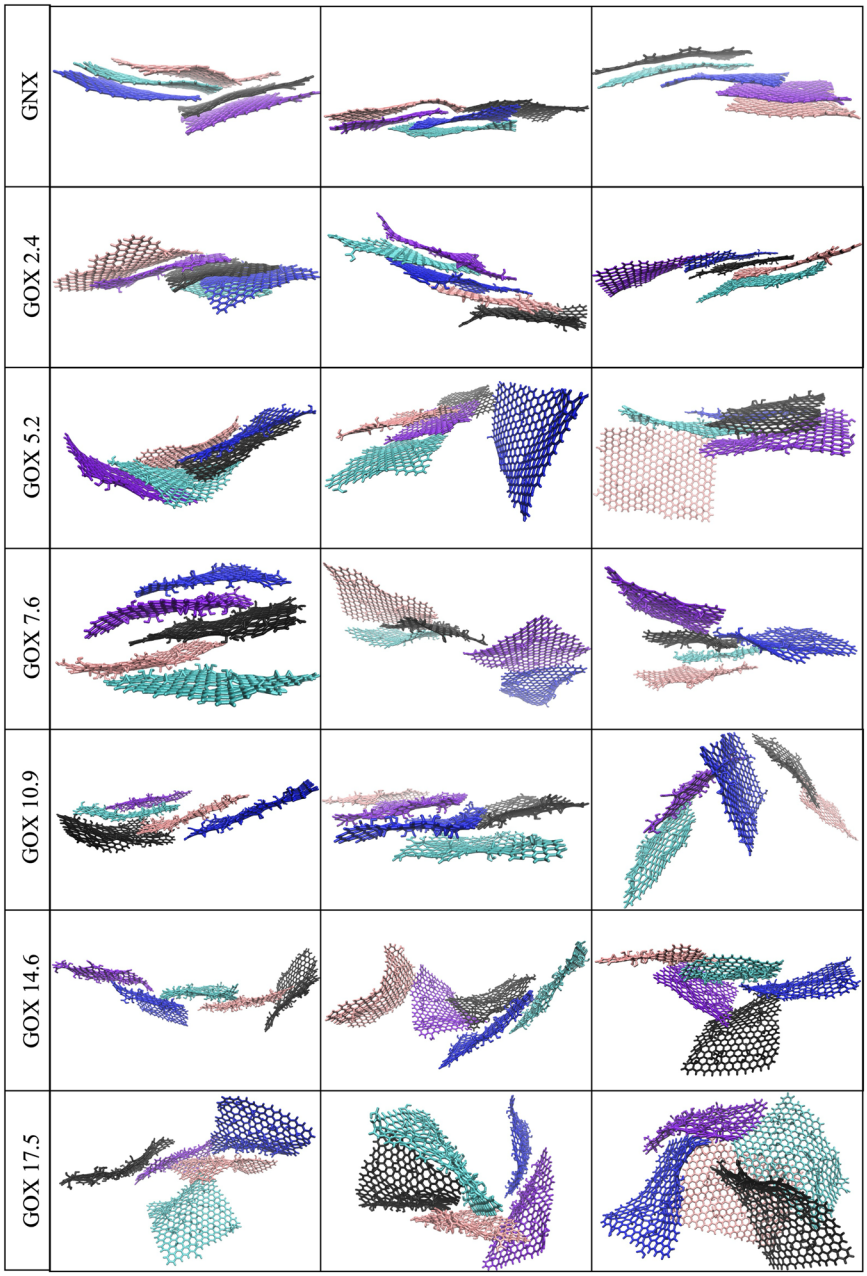

Fig. 6 Snapshot from the last step of three configurations of simulations. Flakes are shown in different colors to visualize how the flakes interact with each other.

PFBA. For GOX 2.4, the long chain PFAS tail groups are 10 times more likely to be 4–6 Å from the carbon backbone than in solution. These curves are essentially identical. For GOX 5.2, the PFOA tail group peak has increased to 11, while PFOS is 12 times more likely to be near the backbone. As the oxygen coverage increases above 7.6% oxygen by weight, the PFOA adsorption diminishes more rapidly than the PFOS adsorption. This is likely due to the spacing increasing between flakes, and pockets forming for PFAS tails to sit in. The PFOS molecules are slightly less soluble in water than PFOA. The PFOS will find and adsorb to limited hydrophobic regions more competitively than PFOA. There is a decrease in propensity for the PFAS tail group to be near the backbone at ≥10.9% oxygen by weight. This is in line with the observations made with the PFAS–flake LIE results. As the oxygen level increases, there is less interaction between the hydrophobic PFAS tail and the surface of the flake. There is low likelihood for the PFBA to be near the carbon backbone of all flakes.

Interestingly, there is some affinity for the head group of the long chain PFAS to be near the carbon backbone. The PFOS head group is 11.5 times more likely to be 4–6 Å from the carbon backbone than in solution for GOX 5.2. As the oxygen level increases, the peak splits into two modes.

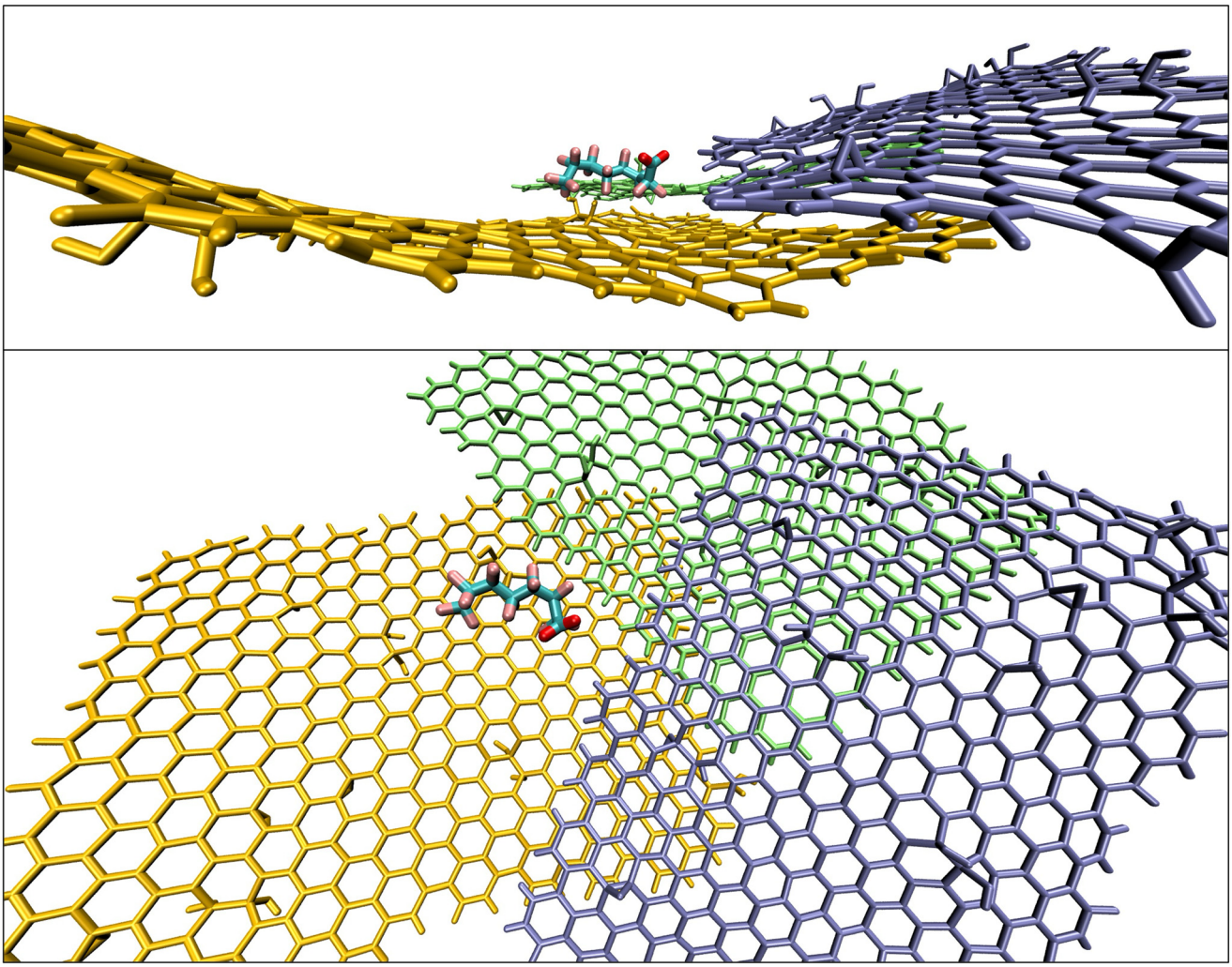

Fig. 7 Snapshot of PFOA interacting at the shelf/hydrophilic edge intersection of three GOX 5.2 flakes.

Trajectories were visually examined to explain this phenomenon. For GOX 5.2, the PFOS tail prefers to be located over the carbon backbone. The shelves made by the flake clustering allow the head group of the PFOS to interact with the hydrogen border of the flake, while the tail rests on the carbon surface of the shelf. These PFOS lay flat on the surface of the shelf, with the headgroup interacting with the edge. Thus, the PFOS head group is still in close proximity to the carbon backbone. Further, PFOS is likely to orient around the intersection of two flakes and interacts with the backbone of two flakes, placing the head group near the carbon backbone of both flakes. As the oxygen level increases, the PFOS stays near the intersection, but the flakes spread out, creating the bimodal peak starting in GOX 7.6, and clearly seen in GOX 10.9, GOX 14.6 and GOX 17.5.

3.4. Hydroxyl RDFs

Fig. 9 shows the RDFs for PFAS interacting with the hydroxyl groups of graphene oxide. The RDFs become less noisy as more oxygen groups are added. PFOA and PFBA head groups have little affinity for the hydroxyl group. There is some propensity for PFOS to be near the hydroxyl groups, but it decreases after GOX 10.9. However, the tail group of PFOS and PFOA has a much stronger affinity for the hydroxyl groups than the head groups. This phenomenon is counterintuitive, and so trajectories were visualized to determine the cause. The hydroxyl groups act as an interaction site between flakes. GOX 5.2 and GOX 7.6 seem to have an ideal interaction between flakes creating shelves and pockets for the capture of PFAS. As the PFAS interact with the flakes at agglomeration sites, the PFAS tail groups interact strongly with hydrophobic surfaces of two flakes. Thus, the PFAS is tightly bound to an agglomeration site and the tail of the PFAS is near a hydroxyl group. The strong affinity of the PFAS tail group for the hydroxyl groups of the graphene oxide is a byproduct of flake stacking, orientation, and proximity of OH groups around the carbon backbone. As the oxidation levels continue to increase towards 17.5% oxygen by mass, the PFAS

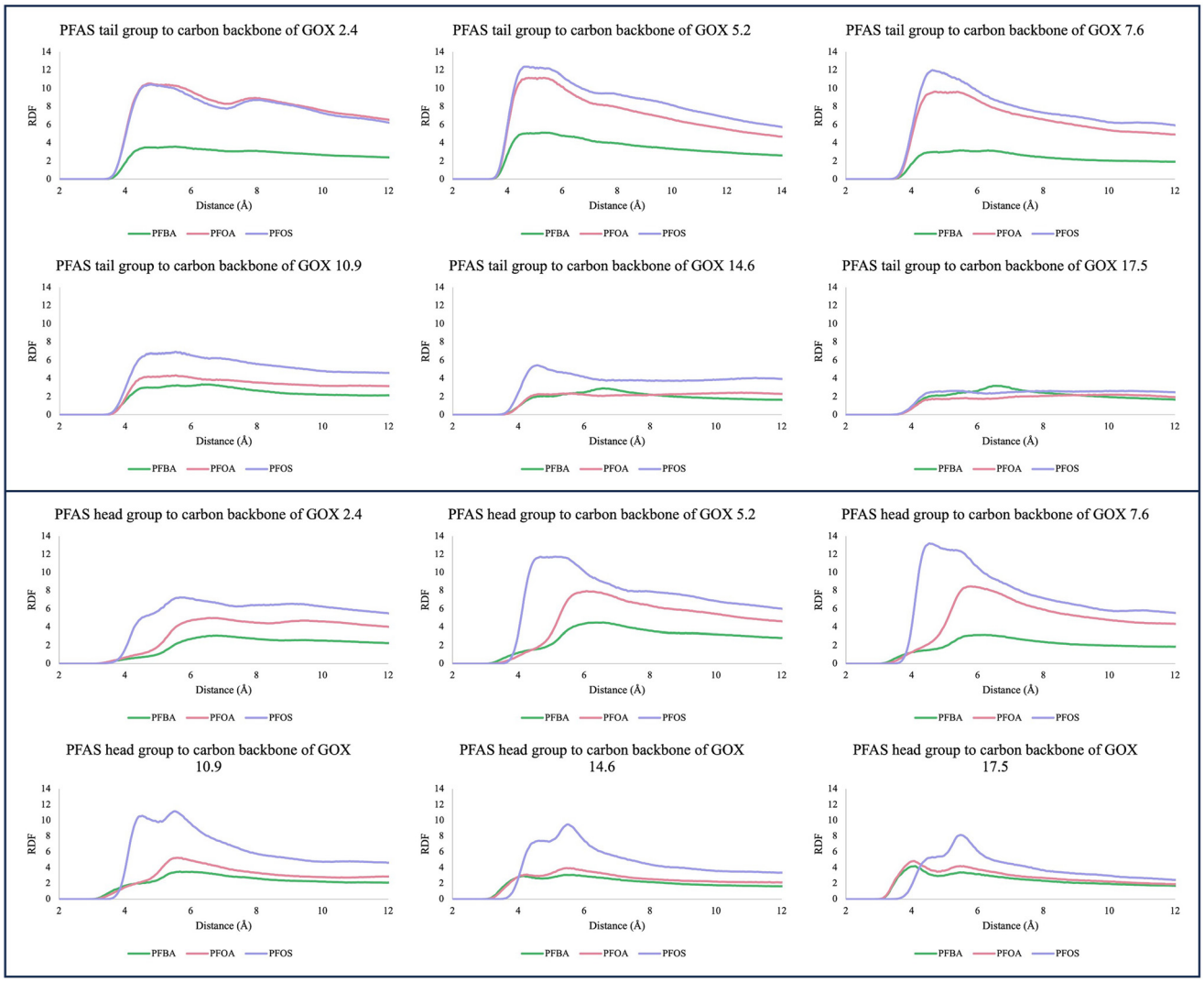

Fig. 8 Top panel – RDFs of the PFAS tail group to the carbon backbone. Bottom panel – RDFs of the PFAS head group to the carbon backbone.

interaction with hydroxyls diminishes significantly due to reduced flake–flake stacking interaction and the existence of only a few neighboring hydrophobic carbon backbone sites.

3.5. Flake hydrogen border edge RDFs

All of the flakes have a hydrogen border. The hydrogen border acts as an interaction site between graphene oxide flakes as can be seen in Fig. 5 and 6. When shelves were formed in GOX 2.4–7.6, the edge of the shelf is the hydrogen border of the flakes. The head group of the PFAS interacts with the hydrogen border of the edge of one flake while the tail group lies flat over the hydrophobic carbon backbone of the same flake, or an adjacent flake. This phenomenon is most pronounced in the GNX results. Fig. 10 shows the RDFs of the PFAS head group to the hydrogen border. As with the carbon backbone, lower broad peaks are expected due to the spread-out nature of the hydrogen border compared to other functional groups. RDFs for the tail group are shown in Fig. S6. With GNX, the PFOS head group is 16 times more likely to be 4–5 Å from hydrogen border than in solution. For PFOA, it is 14 times more likely to be 5 Å from the hydrogen border than in solution. The snapshots of GNX in Fig. 4 show that PFAS interacts near the hydrogen borders of the flake, while the tail group often interacts with the carbon backbone. PFOA and PFOS continue to be 9–10 times more likely to be 5–6 Å away from the hydrogen border at GOX 2.4 and GOX 5.2. PFOS is 8–10 times more likely to be 4.5 to 6 Å away from the hydrogen border as the oxygen level increases. The composite picture between the flake–flake interactions and the RDFs shows that the flakes cluster to form shelves and pockets. PFOA and PFOS tail groups interact with the carbon backbone of the flake while the head group prefers to be around the hydrogen border or, to a lesser extent, a hydroxyl group. GOX 5.2 and GOX 7.6 have the

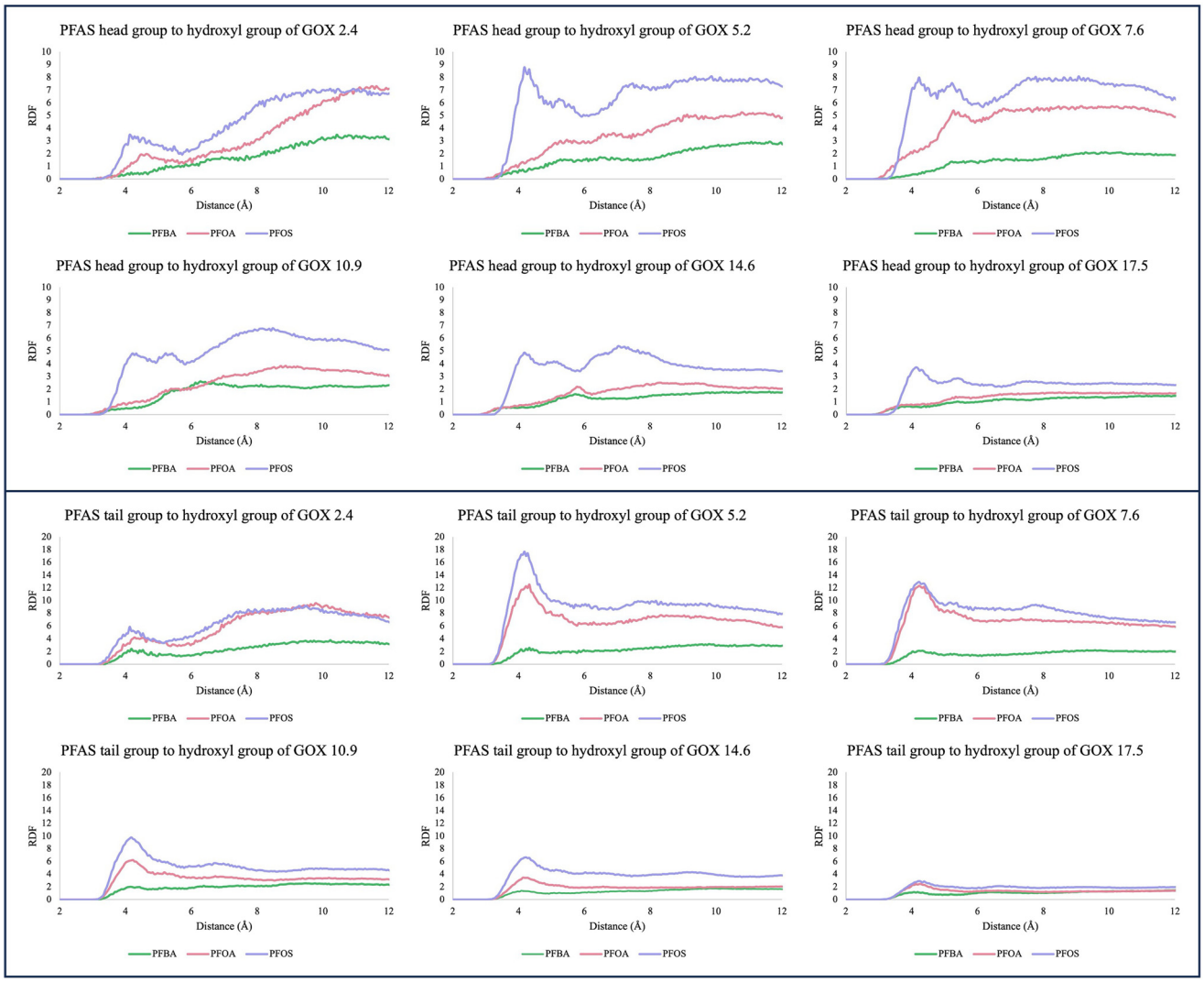

Fig. 9 Top panel – RDFs of the PFAS head group to hydroxyl group of flakes. Bottom panel – RDFs for the tail group to hydroxyl group of flakes.

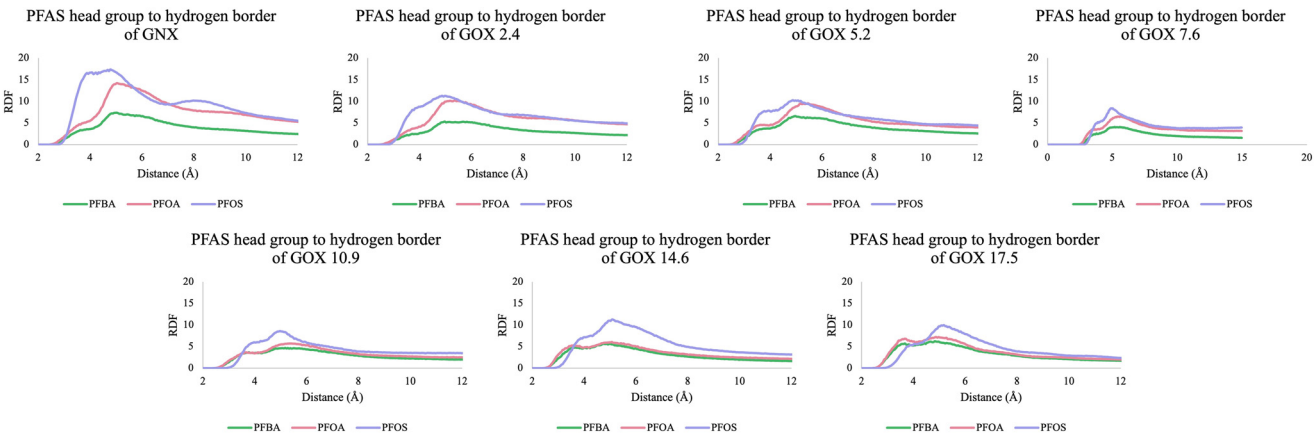

Fig. 10 RDFs of the head group of PFAS to the hydrogen border of the graphene oxide flakes.

best interplay of retaining hydrophobic surfaces in each flake, enough oxygen coverage to form high-surface-area flake aggregates, and hydrated regions for the interaction of PFAS head groups.

4. Conclusions

This work examined how changing the oxygen coverage of a graphene oxide flake impacts flake aggregation and PFAS capture. In particular, it illuminated the interplay between electrostatic interactions and hydrophobic effects at the molecular level, and how those parameters can be leveraged to optimize PFAS binding. Seven graphene oxide flakes ranging from 0.0% to 17.5% oxygen by weight were examined. It was found that PFOA and PFOS have similar interactions with graphene oxide until GOX 10.9. PFOS and PFOA interactions with the flake decrease at GOX 10.9 and continue to decrease as oxygen coverage increases. The strength of the interaction decreases more quickly for PFOA than PFOS. GOX 5.2 and GOX 7.6 perform the best for PFAS capture. This is due to a favorable mixture of several components: 1) PFAS headgroup electrostatic interactions with the functional groups on the flake, 2) hydrophobic effects leading to the PFAS tail laying over the hydrophobic backbone of the flakes, and 3) ideal flake separation due to interactions between functional groups and hydrophobic backbones. GOX 5.2 has more shelf off-set stacked flakes while GOX 7.6 has more pockets for PFAS to interact with. At these low oxygen coverages, there are enough oxygen groups to allow for high surface area clustering to occur while the hydrophobic carbon backbone is available to interact with PFAS tail groups. As the oxygen level increases, the flake–flake interaction and available surface area plateau. However, the increase in hydrophilic oxygen groups reduces the hydrophobic carbon backbone availability, decreasing their aptitude for capturing PFAS.

Author contributions

Caitlin G. Bresnahan: conceptualization, analysis, investigation, methodology, writing. Timothy C. Schutt: conceptualization, writing – review and editing. Manoj K. Shukla: project administration, resources, supervision, writing – review and editing.

Conflicts of interest

There are no conflicts of interest to declare.

Data availability

Data available on request from authors.

Supplementary information (SI) is available. See DOI: https://doi.org/10.1039/d5en00731c.

Acknowledgements

The use of trade, product, or firm names in this report is for descriptive purposes only and does not imply endorsement by the U.S. Government. The tests described and the resulting data presented herein, unless otherwise noted, were obtained from research funded under the Installations and Operational Environments, Office of the Technical Director of the United States Army Corps of Engineers, Engineer Research and Development Center, Environmental Laboratory. Permission was granted by the Chief of Engineers to publish this information. The findings of this report are not to be considered as an official Department of the Army position unless so designated by other authorized documents. This work was supported by a grant of computer time from the DoD High Performance Computing Modernization Program at US Army ERDC, Vicksburg, MS. This document has been approved for public release (Distribution Statement A).

References

1 S. C. E. Leung, D. Wanninayake, D. Chen, N.-T. Nguyen and Q. Li, Physicochemical properties and interactions of perfluoroalkyl substances (PFAS) - Challenges and opportunities in sensing and remediation, *Sci. Total Environ.*, 2023, **905**, 166764, DOI: 10.1016/j.scitotenv.2023.166764.

2 S. V. A. C. Samarasinghe, A. Wijayawardena, A. U. H. Khan, Y. Liu and R. Naidu, *Per- and Polyfluorinated Alkyl Substances: Occurrence, Toxicity and Remediation of PFAS*, De Gruyter, 2025, DOI: 10.1515/9783110796797.

3 D. C. Perera and J. N. Meegoda, PFAS: The Journey from Wonder Chemicals to Environmental Nightmares and the Search for Solutions, *Appl. Sci.*, 2024, **14**, 8611.

4 L. G. T. Gaines, Historical and current usage of per- and polyfluoroalkyl substances (PFAS): A literature review, *Am. J. Ind. Med.*, 2023, **66**(5), 353–378, DOI: 10.1002/ajim.23362.

5 Y. Fujii, K. H. Harada and A. Koizumi, Occurrence of perfluorinated carboxylic acids (PFCAs) in personal care products and compounding agents, *Chemosphere*, 2013, **93**(3), 538–544, DOI: 10.1016/j.chemosphere.2013.06.049.

6 J. Glüge, M. Scheringer, I. T. Cousins, J. C. DeWitt, G. Goldenman, D. Herzke, R. Lohmann, C. A. Ng, X. Trier and Z. Wang, An overview of the uses of per- and polyfluoroalkyl substances (PFAS), *Environ. Sci.: Processes Impacts*, 2020, **22**(12), 2345–2373, DOI: 10.1039/D0EM00291G.

7 Z. Habib, M. Song, S. Ikram and Z. Zahra, Overview of Per- and Polyfluoroalkyl Substances (PFAS), Their Applications, Sources, and Potential Impacts on Human Health, *Pollutants*, 2024, **4**, 136–152.

8 J. T. Thompson, B. Chen, J. A. Bowden and T. G. Townsend, Per- and Polyfluoroalkyl Substances in Toilet Paper and the Impact on Wastewater Systems, *Environ. Sci. Technol. Lett.*, 2023, **10**(3), 234–239, DOI: 10.1021/acs.estlett.3c00094.

9 P. S. Pauletto and T. J. Bandosz, Activated carbon versus metal-organic frameworks: A review of their PFAS adsorption performance, *J. Hazard. Mater.*, 2022, **425**, 127810, DOI: 10.1016/j.jhazmat.2021.127810.

10 J. E. Galloway, A. V. P. Moreno, A. B. Lindstrom, M. J. Strynar, S. Newton, A. A. May and L. K. Weavers, Evidence of Air Dispersion: HFPO–DA and PFOA in Ohio and West Virginia Surface Water and Soil near a Fluoropolymer

Production Facility, *Environ. Sci. Technol.*, 2020, **54**(12), 7175–7184, DOI: 10.1021/acs.est.9b07384.

11 M. N. Ehsan, M. Riza, M. N. Pervez, M. M. O. Khyum, Y. Liang and V. Naddeo, Environmental and health impacts of PFAS: Sources, distribution and sustainable management in North Carolina (USA), *Sci. Total Environ.*, 2023, **878**, 163123, DOI: 10.1016/j.scitotenv.2023.163123.

12 L. Ahrens, J. Rakovic, S. Ekdahl and R. Kallenborn, Environmental distribution of per- and polyfluoroalkyl substances (PFAS) on Svalbard: Local sources and long-range transport to the Arctic, *Chemosphere*, 2023, **345**, 140463, DOI: 10.1016/j.chemosphere.2023.140463.

13 S. P. Lenka, M. Kah and L. P. Padhye, A review of the occurrence, transformation, and removal of poly- and perfluoroalkyl substances (PFAS) in wastewater treatment plants, *Water Res.*, 2021, **199**, 117187, DOI: 10.1016/j.watres.2021.117187.

14 N. H. Lam, C.-R. Cho, K. Kannan and H.-S. Cho, A nationwide survey of perfluorinated alkyl substances in waters, sediment and biota collected from aquatic environment in Vietnam: Distributions and bioconcentration profiles, *J. Hazard. Mater.*, 2017, **323**, 116–127, DOI: 10.1016/j.jhazmat.2016.04.010.

15 A. Shankar, J. Xiao and A. Ducatman, Perfluoroalkyl Chemicals and Chronic Kidney Disease in US Adults, *Am. J. Epidemiol.*, 2011, **174**(8), 893–900, DOI: 10.1093/aje/kwr171.

16 M.-J. Lopez-Espinosa, D. Mondal, B. Armstrong, S. Bloom Michael and T. Fletcher, Thyroid Function and Perfluoroalkyl Acids in Children Living Near a Chemical Plant, *Environ. Health Perspect.*, 2012, **120**(7), 1036–1041, DOI: 10.1289/ehp.1104370.

17 V. Barry, A. Winquist and K. Steenland, Perfluorooctanoic Acid (PFOA) Exposures and Incident Cancers among Adults Living Near a Chemical Plant, *Environ. Health Perspect.*, 2013, **121**(11–12), 1313–1318, DOI: 10.1289/ehp.1306615.

18 C. R. Stein, K. J. McGovern, A. M. Pajak, P. J. Maglione and M. S. Wolff, Perfluoroalkyl and polyfluoroalkyl substances and indicators of immune function in children aged 12–19 y: National Health and Nutrition Examination Survey, *Pediatr. Res.*, 2016, **79**(2), 348–357, DOI: 10.1038/pr.2015.213.

19 L. Li, Y. Guo, S. Ma, H. Wen, Y. Li and J. Qiao, Association between exposure to per- and perfluoroalkyl substances (PFAS) and reproductive hormones in human: A systematic review and meta-analysis, *Environ. Res.*, 2024, **241**, 117553, DOI: 10.1016/j.envres.2023.117553.

20 S. India-Aldana, M. Yao, V. Midya, E. Colicino, L. Chatzi, J. Chu, C. Gennings, D. P. Jones, R. J. F. Loos and V. W. Setiawan, *et al.*, PFAS Exposures and the Human Metabolome: A Systematic Review of Epidemiological Studies, *Curr. Pollut. Rep.*, 2023, **9**(3), 510–568, DOI: 10.1007/s40726-023-00269-4.

21 I. A. L. P. van Beijsterveldt, B. D. van Zelst, K. S. de Fluiter, S. A. A. van den Berg, M. van der Steen and A. C. S. Hokken-Koelega, Poly- and perfluoroalkyl substances (PFAS) exposure through infant feeding in early life, *Environ. Int.*, 2022, **164**, 107274, DOI: 10.1016/j.envint.2022.107274.

22 Perfluoroalkyl and Polyfluoroalkyl Substances (PFAS), https://www.niehs.nih.gov/health/topics/agents/pfc, (accessed 2025 June).

23 T. Jiang, W. Zhang, A. K. Ilango, J. I. Feldblyum, Z. Wei, H. Efstathiadis, M. V. Yigit and Y. Liang, Surfactant-Modified Clay for Adsorption of Mixtures of Per- and Polyfluoroalkyl Substances (PFAS) in Aqueous Solutions, *ACS Appl. Eng. Mater.*, 2023, **1**(1), 394–407, DOI: 10.1021/acsaenm.2c00096.

24 N. Loganathan and A. K. Wilson, Adsorption, Structure, and Dynamics of Short- and Long-Chain PFAS Molecules in Kaolinite: Molecular-Level Insights, *Environ. Sci. Technol.*, 2022, **56**(12), 8043–8052, DOI: 10.1021/acs.est.2c01054.

25 C. M. Luft, T. C. Schutt and M. K. Shukla, Properties and Mechanisms for PFAS Adsorption to Aqueous Clay and Humic Soil Components, *Environ. Sci. Technol.*, 2022, **56**(14), 10053–10061, DOI: 10.1021/acs.est.2c00499.

26 J. A. R. Willemsen and I. C. Bourg, Molecular dynamics simulation of the adsorption of per- and polyfluoroalkyl substances (PFASs) on smectite clay, *J. Colloid Interface Sci.*, 2021, **585**, 337–346, DOI: 10.1016/j.jcis.2020.11.071.

27 Q. Dong, X. Min, Y. Zhao and Y. Wang, Adsorption of per- and polyfluoroalkyl substances (PFAS) by ionic liquid-modified clays: Effect of clay composition and PFAS structure, *J. Colloid Interface Sci.*, 2024, **654**, 925–934, DOI: 10.1016/j.jcis.2023.10.112.

28 M. Park, S. Wu, I. J. Lopez, J. Y. Chang, T. Karanfil and S. A. Snyder, Adsorption of perfluoroalkyl substances (PFAS) in groundwater by granular activated carbons: Roles of hydrophobicity of PFAS and carbon characteristics, *Water Res.*, 2020, **170**, 115364, DOI: 10.1016/j.watres.2019.115364.

29 B. Cantoni, A. Turolla, J. Wellmitz, A. S. Ruhl and M. Antonelli, Perfluoroalkyl substances (PFAS) adsorption in drinking water by granular activated carbon: Influence of activated carbon and PFAS characteristics, *Sci. Total Environ.*, 2021, **795**, 148821, DOI: 10.1016/j.scitotenv.2021.148821.

30 Y. Zhang, A. Thomas, O. Apul and A. K. Venkatesan, Coexisting ions and long-chain per- and polyfluoroalkyl substances (PFAS) inhibit the adsorption of short-chain PFAS by granular activated carbon, *J. Hazard. Mater.*, 2023, **460**, 132378, DOI: 10.1016/j.jhazmat.2023.132378.

31 G. Kim, D. N. Mengesha and Y. Choi, Adsorption dynamics of per- and polyfluoroalkyl substances (PFAS) on activated carbon: Interplay of surface chemistry and PFAS structural properties, *Sep. Purif. Technol.*, 2024, **349**, 127851, DOI: 10.1016/j.seppur.2024.127851.

32 H. Son and B. An, Investigation of Adsorption Kinetics for Per- and Poly-fluoroalkyl substances (PFAS) Adsorption onto Powder Activated Carbon (PAC) in the Competing Systems, *Water, Air, Soil Pollut.*, 2022, **233**(4), 129, DOI: 10.1007/s11270-022-05599-5.

33 H. Son, T. Kim, H.-S. Yoom, D. Zhao and B. An, The Adsorption Selectivity of Short and Long Per- and Polyfluoroalkyl Substances (PFASs) from Surface Water Using Powder-Activated Carbon, *Water*, 2020, **12**, 3287.

34 M. Ateia, M. F. Attia, A. Maroli, N. Tharayil, F. Alexis, D. C. Whitehead and T. Karanfil, Rapid Removal of Poly- and

Perfluorinated Alkyl Substances by Poly(ethylenimine)-Functionalized Cellulose Microcrystals at Environmentally Relevant Conditions, *Environ. Sci. Technol. Lett.*, 2018, **5**(12), 764–769, DOI: 10.1021/acs.estlett.8b00556.

35 D. Li, R. Das, Y. Zhang, S. Zheng, M. Oltulu, A. K. Venkatesan and B. S. Hsiao, Alkylamine-Modified Dialdehyde Cellulose Nanofibers for PFAS Adsorption, *ACS ES&T Water*, 2025, **5**(4), 1582–1594, DOI: 10.1021/acsestwater.4c00870.

36 G.-W. Hu, J.-H. Zhao, B. Liu, N.-L. Xiao, H.-D. Wang, M. Zhang, Q. Li, P.-Y. Li and H.-J. Lai, Preparation of nylon-6 modified cellulose paper for extraction and determination of perfluoroalkyl substances in water, *Ind. Crops Prod.*, 2024, **212**, 118263, DOI: 10.1016/j.indcrop.2024.118263.

37 P. Chularueangaksorn, S. Tanaka, S. Fujii and C. Kunacheva, Regeneration and reusability of anion exchange resin used in perfluorooctane sulfonate removal by batch experiments, *J. Appl. Polym. Sci.*, 2013, **130**(2), 884–890, DOI: 10.1002/app.39169.

38 P. Chularueangaksorn, S. Tanaka, S. Fujii and C. Kunacheva, Adsorption of perfluorooctanoic acid (PFOA) onto anion exchange resin, non-ion exchange resin, and granular-activated carbon by batch and column, *Desalin. Water Treat.*, 2014, **52**(34), 6542–6548, DOI: 10.1080/19443994.2013.815589.

39 F. Dixit, R. Dutta, B. Barbeau, P. Berube and M. Mohseni, PFAS removal by ion exchange resins: A review, *Chemosphere*, 2021, **272**, 129777, DOI: 10.1016/j.chemosphere.2021.129777.

40 M. Zhang and A. O. Yazaydin, The effect of perfluoroalkyl chain length and the type of acid group on PFAS adsorption from water, *Chem. Eng. J.*, 2024, **499**, 155851, DOI: 10.1016/j.cej.2024.155851.

41 A. Lauwers, J. Vercammen and D. De Vos, Adsorption of PFAS by All-Silica Zeolite β: Insights into the Effect of the Water Matrix, Regeneration of the Material, and Continuous PFAS Adsorption, *ACS Appl. Mater. Interfaces*, 2023, **15**(45), 52612–52621, DOI: 10.1021/acsami.3c12321.

42 C. A. Ponge, N. P. Sheehan, D. R. Corbin, E. Peltier, J. M. Hutchison and M. B. Shiflett, Zeolites for Sorption of PFAS from Water, *Ind. Eng. Chem. Res.*, 2024, **63**(27), 12102–12112, DOI: 10.1021/acs.iecr.4c00541.

43 Y. Yang, Z. Zheng, W. Ji, J. Xu and X. Zhang, Insights to perfluorooctanoic acid adsorption micro-mechanism over Fe-based metal organic frameworks: Combining computational calculation with response surface methodology, *J. Hazard. Mater.*, 2020, **395**, 122686, DOI: 10.1016/j.jhazmat.2020.122686.

44 D. Barpaga, J. Zheng, K. S. Han, J. A. Soltis, V. Shutthanandan, S. Basuray, B. P. McGrail, S. Chatterjee and R. K. Motkuri, Probing the Sorption of Perfluorooctanesulfonate Using Mesoporous Metal–Organic Frameworks from Aqueous Solutions, *Inorg. Chem.*, 2019, **58**(13), 8339–8346, DOI: 10.1021/acs.inorgchem.9b00380.

45 N. Ilić, K. Tan, F. Mayr, S. Hou, B. M. Aumeier, E. M. C. Morales, U. Hübner, J. Cookman, A. Schneemann and A. Gagliardi, *et al.*, Trace Adsorptive Removal of PFAS from Water by Optimizing the UiO-66 MOF Interface, *Adv. Mater.*, 2025, **37**(6), 2413120, DOI: 10.1002/adma.202413120.

46 Z. Liu, M. Liao, L. Wang and S. Zhuang, Recent advancements in PFAS adsorptive removal using MOFs and COFs: a review, *Rev. Environ. Sci. Bio/Technol.*, 2025, **24**(1), 63–95, DOI: 10.1007/s11157-024-09715-1.

47 X. Song, R. Wang, X. Wang, H. Han, Z. Qiao, X. Sun and W. Ji, An amine-functionalized olefin-linked covalent organic framework used for the solid-phase microextraction of legacy and emerging per- and polyfluoroalkyl substances in fish, *J. Hazard. Mater.*, 2022, **423**, 127226, DOI: 10.1016/j.jhazmat.2021.127226.

48 A. Zarei, A. Khosropour, L. Khazdooz, S. Amirjalayer, A. Khojastegi, A. Zadehnazari, Y. Zhao and A. Abbaspourrad, Substitution and Orientation Effects on the Crystallinity and PFAS Adsorption of Olefin-Linked 2D COFs, *ACS Appl. Mater. Interfaces*, 2024, **16**(7), 9483–9494, DOI: 10.1021/acsami.3c17188.

49 A. Choudhary and D. Bedrov, Interaction of Short-Chain PFAS with Polycationic Gels: How Much Fluorination is Necessary for Efficient Adsorption?, *ACS Macro Lett.*, 2022, **11**(9), 1123–1128, DOI: 10.1021/acsmacrolett.2c00383.

50 E. Kumarasamy, I. M. Manning, L. B. Collins, O. Coronell and F. A. Leibfarth, Ionic Fluorogels for Remediation of Per- and Polyfluorinated Alkyl Substances from Water, *ACS Cent. Sci.*, 2020, **6**(4), 487–492, DOI: 10.1021/acscentsci.9b01224.

51 J. Wang, Q. Qi, Y. Ji, X. Liu and Q. Shi, Thermosensitive hydrogels for efficient removal of perfluorooctanesulfonic acid, *Mater. Lett.*, 2025, **382**, 137886, DOI: 10.1016/j.matlet.2024.137886.

52 A. Choudhary, D. Dong, M. Tsianou, P. Alexandridis and D. Bedrov, Adsorption Mechanism of Perfluorooctanoate on Cyclodextrin-Based Polymers: Probing the Synergy of Electrostatic and Hydrophobic Interactions with Molecular Dynamics Simulations, *ACS Mater. Lett.*, 2022, **4**(5), 853–859, DOI: 10.1021/acsmaterialslett.2c00168.

53 A. Yang, C. Ching, M. Easler, D. E. Helbling and W. R. Dichtel, Cyclodextrin Polymers with Nitrogen-Containing Tripodal Crosslinkers for Efficient PFAS Adsorption, *ACS Mater. Lett.*, 2020, **2**(9), 1240–1245, DOI: 10.1021/acsmaterialslett.0c00240.

54 E. Gagliano, M. Sgroi, P. P. Falciglia, F. G. A. Vagliasindi and P. Roccaro, Removal of poly- and perfluoroalkyl substances (PFAS) from water by adsorption: Role of PFAS chain length, effect of organic matter and challenges in adsorbent regeneration, *Water Res.*, 2020, **171**, 115381, DOI: 10.1016/j.watres.2019.115381.

55 X. Lei, Q. Lian, X. Zhang, T. K. Karsili, W. Holmes, Y. Chen, M. E. Zappi and D. D. Gang, A review of PFAS adsorption from aqueous solutions: Current approaches, engineering applications, challenges, and opportunities, *Environ. Pollut.*, 2023, **321**, 121138, DOI: 10.1016/j.envpol.2023.121138.

56 B. Shrestha, M. Ezazi, S. Ajayan and G. Kwon, Reversible adsorption and desorption of PFAS on inexpensive graphite adsorbents via alternating electric field, *RSC Adv.*, 2021, **11**(55), 34652–34659, DOI: 10.1039/D1RA04821J.

57 X. Wang, H. Zhang, S. Ham and R. Qiao, Graphene Oxide and Its Derivatives as Adsorbents for PFOA Molecules, *J. Phys. Chem. B*, 2023, **127**(44), 9620–9629, DOI: 10.1021/acs.jpcb.3c04762.
58 M. N. Pervez, T. Jiang, J. K. Mahato, A. K. Ilango, Y. Kumaran, Y. Zuo, W. Zhang, H. Efstathiadis, J. I. Feldblyum and M. V. Yigit, *et al.*, Surface Modification of Graphene Oxide for Fast Removal of Per- and Polyfluoroalkyl Substances (PFAS) Mixtures from River Water, *ACS ES&T Water*, 2024, **4**(7), 2968–2980, DOI: 10.1021/acsestwater.4c00187.
59 A. H. Behroozi, L. Meunier, A. Mirahsani, P. Champagne and E. H. Koupaie, Graphene-based materials and technologies for the treatment of PFAS in water: A review of recent developments, *J. Hazard. Mater. Adv.*, 2025, **17**, 100626, DOI: 10.1016/j.hazadv.2025.100626.
60 B. G. Lamb and B. Ma, PFAS self-assembly and adsorption dynamics on graphene: molecular insights into chemical and environmental influences, *Nanoscale*, 2025, **17**(17), 10632–10643, DOI: 10.1039/D4NR04995K.
61 A. Trifoglio, S. Mantovani, S. Khaliha, A. Kovtun, T. D. Marforio, M. Calvaresi and M. Melucci, Tailoring graphene oxide nanosheets by alkyl amine grafting for enhanced adsorption of PFASs in drinking water: a combined theoretical and experimental study, *Nanoscale*, 2025, **17**(19), 12124–12133, DOI: 10.1039/D5NR00502G.
62 C. G. Bresnahan, T. C. Schutt and M. K. Shukla, Exploration of functionalizing graphene and the subsequent impact on PFAS adsorption capabilities via molecular dynamics, *Chemosphere*, 2023, **345**, 140462, DOI: 10.1016/j.chemosphere.2023.140462.
63 C. G. Bresnahan, T. C. Schutt and M. K. Shukla, A molecular dynamics investigation into manipulating graphene flake spacing for increased selectivity towards short chain PFAS capture, *Chemosphere*, 2025, **373**, 144135, DOI: 10.1016/j.chemosphere.2025.144135.
64 S. Mahpishanian, M. Zhou and R. Foudazi, Magnetic amino-functionalized graphene oxide nanocomposite for PFAS removal from water, *Environ. Sci.: Adv.*, 2024, **3**(12), 1698–1713, DOI: 10.1039/D4VA00171K.
65 S. Lath, D. A. Navarro, D. Losic, A. Kumar and M. J. McLaughlin, Sorptive remediation of perfluorooctanoic acid (PFOA) using mixed mineral and graphene/carbon-based materials, *Environ. Chem.*, 2018, **15**(8), 472–480.
66 N. Saeidi, A. Lai, F. Harnisch and G. Sigmund, A FAIR comparison of activated carbon, biochar, cyclodextrins, polymers, resins, and metal organic frameworks for the adsorption of per- and polyfluorinated substances, *Chem. Eng. J.*, 2024, **498**, 155456, DOI: 10.1016/j.cej.2024.155456.
67 J. Fabregat-Palau, M. Vidal and A. Rigol, Examining sorption of perfluoroalkyl substances (PFAS) in biochars and other carbon-rich materials, *Chemosphere*, 2022, **302**, 134733, DOI: 10.1016/j.chemosphere.2022.134733.
68 B. Anegbe, I. H. Ifijen, M. Maliki, I. E. Uwidia and A. I. Aigbodion, Graphene oxide synthesis and applications in emerging contaminant removal: a comprehensive review, *Environ. Sci. Eur.*, 2024, **36**(1), 15, DOI: 10.1186/s12302-023-00814-4.
69 F. Asghar, B. Shakoor, S. Fatima, S. Munir, H. Razzaq, S. Naheed and I. S. Butler, Fabrication and prospective applications of graphene oxide-modified nanocomposites for wastewater remediation, *RSC Adv.*, 2022, **12**(19), 11750–11768, DOI: 10.1039/D2RA00271J.
70 A. J. Paulista Neto and E. E. Fileti, Elucidating the amphiphilic character of graphene oxide, *Phys. Chem. Chem. Phys.*, 2018, **20**(14), 9507–9515, DOI: 10.1039/C8CP00797G.
71 J. Kim, L. J. Cote and J. Huang, Two Dimensional Soft Material: New Faces of Graphene Oxide, *Acc. Chem. Res.*, 2012, **45**(8), 1356–1364, DOI: 10.1021/ar300047s.
72 S. Radic, N. K. Geitner, R. Podila, A. Käkinen, P. Chen, P. C. Ke and F. Ding, Competitive Binding of Natural Amphiphiles with Graphene Derivatives, *Sci. Rep.*, 2013, **3**(1), 2273, DOI: 10.1038/srep02273.
73 K. Krishnamoorthy, M. Veerapandian, K. Yun and S. J. Kim, The chemical and structural analysis of graphene oxide with different degrees of oxidation, *Carbon*, 2013, **53**, 38–49, DOI: 10.1016/j.carbon.2012.10.013.
74 I. Karnis, F. Krasanakis, L. Sygellou, A. N. Rissanou, K. Karatasos and K. Chrissopoulou, Varying the degree of oxidation of graphite: effect of oxidation time and oxidant mass, *Phys. Chem. Chem. Phys.*, 2024, **26**(13), 10054–10068, DOI: 10.1039/D3CP05268K.
75 A. Carvalho, M. C. F. Costa, V. S. Marangoni, P. R. Ng, T. L. Nguyen and A. H. Castro Neto, The Degree of Oxidation of Graphene Oxide, *Nanomaterials*, 2021, **11**, 560.
76 C. K. Chua and M. Pumera, Chemical reduction of graphene oxide: a synthetic chemistry viewpoint, *Chem. Soc. Rev.*, 2014, **43**(1), 291–312, DOI: 10.1039/C3CS60303B.
77 W. Liu and G. Speranza, Tuning the Oxygen Content of Reduced Graphene Oxide and Effects on Its Properties, *ACS Omega*, 2021, **6**(9), 6195–6205, DOI: 10.1021/acsomega.0c05578.
78 F. Mouhat, F.-X. Coudert and M.-L. Bocquet, Structure and chemistry of graphene oxide in liquid water from first principles, *Nat. Commun.*, 2020, **11**(1), 1566, DOI: 10.1038/s41467-020-15381-y.
79 J. Wang, R. M. Wolf, J. W. Caldwell, P. A. Kollman and D. A. Case, Development and testing of a general amber force field, *J. Comput. Chem.*, 2004, **25**(9), 1157–1174, DOI: 10.1002/jcc.20035.
80 W. L. Jorgensen, J. Chandrasekhar, J. D. Madura, R. W. Impey and M. L. Klein, Comparison of simple potential functions for simulating liquid water, *J. Chem. Phys.*, 1983, **79**(2), 926–935, DOI: 10.1063/1.445869.
81 H. W. Horn, W. C. Swope, J. W. Pitera, J. D. Madura, T. J. Dick, G. L. Hura and T. Head-Gordon, Development of an improved four-site water model for biomolecular simulations: TIP4P-Ew, *J. Chem. Phys.*, 2004, **120**(20), 9665–9678, DOI: 10.1063/1.1683075.
82 H. W. Horn, W. C. Swope and J. W. Pitera, Characterization of the TIP4P-Ew water model: Vapor pressure and boiling point, *J. Chem. Phys.*, 2005, **123**(19), 194504, DOI: 10.1063/1.2085031.

83 L. Martínez, R. Andrade, E. G. Birgin and J. M. Martínez, PACKMOL: A package for building initial configurations for molecular dynamics simulations, *J. Comput. Chem.*, 2009, **30**(13), 2157–2164, DOI: 10.1002/jcc.21224.

84 D. A. Case, H. M. A, K. Belfon, I. Y. Ben-Shalom, J. T. Berryman, S. R. Brozell, D. S. Cerutti, T. E. Cheatham III, G. A. Cisneros, V. W. D. Cruzeiro, T. A. Darden, R. E. Duke, G. Giambasu, M. K. Gilson, H. Gohlke, A. W. Goetz, R. Harris, S. Izadi, S. A. Izmailov, K. Kasavajhala, M. C. Kaymak, E. King, A. Kovalenko, T. Kurtzman, T. S. Lee, S. LeGrand, P. Li, C. Lin, J. Liu, T. Luchko, R. Luo, M. Machado, V. Man, M. Manathunga, K. M. Merz, Y. Miao, O. Mikhailovskii, G. Monard, H. Nguyen, K. A. O'Hearn, A. Onufriev, F. Pan, S. Pantano, R. Qi, A. Rahnamoun, D. R. Roe, A. Roitberg, C. Sagui, S. Schott-Verdugo, A. Shajan, J. Shen, C. L. Simmerling, N. R. Skrynnikov, J. Smith, J. Swails, R. C. Walker, J. Wang, J. Wang, H. Wei, R. M. Wolf, X. Wu, Y. Xiong, Y. Xue, D. M. York, S. Zhao and P. A. Kollman, *Amber 2022*, University of California, San Francisco, 2022.

85 R. W. Pastor, B. R. Brooks and A. Szabo, An analysis of the accuracy of Langevin and molecular dynamics algorithms, *Mol. Phys.*, 1988, **65**(6), 1409–1419, DOI: 10.1080/00268978800101881.

86 J.-P. Ryckaert, G. Ciccotti and H. J. C. Berendsen, Numerical integration of the cartesian equations of motion of a system with constraints: molecular dynamics of n-alkanes, *J. Comput. Phys.*, 1977, **23**(3), 327–341, DOI: 10.1016/0021-9991(77)90098-5.

87 D. R. Roe and T. E. Cheatham III., PTRAJ and CPPTRAJ: Software for Processing and Analysis of Molecular Dynamics Trajectory Data, *J. Chem. Theory Comput.*, 2013, **9**(7), 3084–3095, DOI: 10.1021/ct400341p.

88 M. L. Connolly, Analytical molecular surface calculation, *J. Appl. Crystallogr.*, 1983, **16**(5), 548–558, DOI: 10.1107/S0021889883010985.

89 W. Humphrey, A. Dalke and K. Schulten, VMD: Visual molecular dynamics, *J. Mol. Graphics*, 1996, **14**(1), 33–38, DOI: 10.1016/0263-7855(96)00018-5.

90 Agency U. S. E. P., Technical Fact Sheet - Perfluorooctane Sulfonate (PFOS) and Perfluorooctanoic acid (PFOA), 2017, https://19january2021snapshot.epa.gov/sites/static/files/2017-12/documents/ffrrofactsheet_contaminants_pfos_pfoa_11-20-17_508_0.pdf, (accessed 2025).

91 Agency for Toxic Substances and Disease Registry (US), Chemical and Physical Information, *Toxicological Profile for Perfluoroalkyls*, 2021, ch. 4, https://www.ncbi.nlm.nih.gov/books/NBK592145/table/ch4.tab2/, (accessed).

